Multipoint observations of coronal mass ejection and solar energetic particle events on Mars and Earth during November 2001

T. V. Falkenberg,[1] S. Vennerstrom,[1] D. A. Brain,[2] G. Delory,[2] and A. Taktakishvili[3]

Received 10 November 2010; revised 4 March 2011; accepted 5 April 2011; published 28 June 2011.

[1] Multipoint spacecraft observations provide unique opportunities to constrain the propagation and evolution of interplanetary coronal mass ejections (ICMEs) throughout the heliosphere. Using Mars Global Surveyor (MGS) data to study both ICME and solar energetic particle (SEP) events at Mars and OMNI and Geostationary Operational Environmental Satellite (GOES) data to study ICMEs and SEPs at Earth, we present a detailed study of three CMEs and flares in late November 2001. In this period, Mars trailed Earth by 56° solar longitude so that the two planets occupied interplanetary magnetic field lines separated by only ~25°. We model the interplanetary propagation of CME events using the ENLIL version 2.6 3-D MHD code coupled with the Wang-Sheeley-Arge version 1.6 potential source surface model, using Solar and Heliospheric Observatory (SOHO) Large Angle and Spectrometric Coronagraph (LASCO) images to determine CME input parameters. We find that multipoint observations are essential to constrain the simulations of ICME propagation, as two very different ICMEs may look very similar in only one observational location. The direction and width of the CME as parameters essential to a correct estimation of arrival time and amplitude of the ICME signal. We find that these are problematic to extract from the analysis of SOHO/LASCO images commonly used for input to ICME propagation models. We further confirm that MGS magnetometer and electron reflectometer data can be used to study not only ICME events but also SEP events at Mars, with good results providing a consistent picture of the events when combined with near-Earth data.

Citation: Falkenberg, T. V., S. Vennerstrom, D. A. Brain, G. Delory, and A. Taktakishvili (2011), Multipoint observations of coronal mass ejection and solar energetic particle events on Mars and Earth during November 2001, *J. Geophys. Res.*, *116*, A06104, doi:10.1029/2010JA016279.

1. Introduction

[2] Predicting the effects of solar eruptions at Earth is currently a major focus area for the space weather community. In particular, prediction of basic parameters such as arrival time and the maximum amplitude of associated solar wind disturbances are of prime importance. These effects are difficult to predict accurately, but recent modeling efforts are showing promise. Successful modeling and forecasting is hampered by two main limitations: the accurate determination of the initial parameters of large solar space weather events is difficult and the physics involved in the origin and the evolution of space weather events is still not completely understood.

[3] The time profiles of various parameters indicative of different types of space weather events, including solar flares, interplanetary coronal mass ejections (ICMEs), and solar energetic particles (SEPs), have been well studied at Earth [e.g., *Reames*, 1999]. However, it is difficult to determine how these events propagate throughout the heliosphere using near-Earth measurements alone. Ideally, multipoint measurements from a variety of solar longitudes and heliocentric distances could be used to constrain propagation. One such opportunity was given by the Helios 1 and 2 spacecraft [*Webb et al.*, 1993; *Schwenn et al.*, 2005], occasionally combined with observations from the IMP [*Reames*,1999] and Voyager spacecraft [*Burlaga et al.*, 1980, 1981]. The STIP (Study of Traveling Interplanetary Phenomena) project encouraged many studies that used Helios 1 and 2, Pioneer-Venus-Orbiter, Venera series, Prognoz series, ISEE-3, Pioneer 10 and 11 and Voyager 1 and 2 [*Dryer and Shea*, 1986], was conducted in the 1980's. It brought together numerous scientist worldwide, an overview of which can be seen by *Dryer* [1987]. More recently, the STEREO A and B spacecraft have observed the Sun and propagating space weather events at 1 AU from different

[1]National Space Institute, Danish Technical University, Lyngby, Denmark.
[2]Space Sciences Laboratory, University of California, Berkeley, California, USA.
[3]NASA Goddard Space Flight Center, Greenbelt, Maryland, USA.

0148-0227/11/2010JA016279

solar longitudes [*Möstl et al.*, 2009; *Lugaz et al.*, 2010; *Zhao et al.*, 2010]. Unfortunately not many large solar events have been observed since their launch in late 2006 due to the prolonged solar minima [*von Rosenvinge et al.*, 2009]. Multipoint studies involving observations from Mars have also been performed recently [*Futaana et al.*, 2008; *McKenna-Lawlor et al.*, 2008; *Crider et al.*, 2005; *Espley et al.*, 2005]; these are described below.

[4] Modeling can provide important context for spacecraft observations, helping to constrain ICME propagation [*Smith and Dryer*, 1990, 1991; *Heras et al.*, 1991]. *Dryer et al.* [2004, references therein] provide a good description and overview of physics-based models. In this study we focus on a simplified version, available through the Community Coordinated Modelling Center (CCMC) at Goddard Space Flight Center, of the ENLIL version 2.6 (ENLILv2.6) model with a cone perturbation [*Odstrcil and Pizzo*, 1999; *Odstrcil et al.*, 2004], which is a 3-D time-dependent numerical magnetohydrodynamic heliospheric model. We use the Wang-Sheeley-Arge version 1.6 (WSAv1.6) model for initial ambient solar wind input. The CME perturbation is initially assumed to be a perfectly uniform front with a user defined angular extent propagating in a cone-like manner. *Taktakishvili et al.* [2009] performed a study of the ENLIL model on 14 selected events, arriving at an average error in arrival time for ICMEs at Earth of ~6 h, but with errors of up to 12 h for individual events (typical propagation times to earth ranging from one to three days). The ENLIL model without a cone perturbation has also been tested against ACE data for the quasi steady state solar wind by *Lee et al.* [2009] and found to be in good agreement, while *Falkenberg et al.* [2010] studied the influence of different input parameters on the ENLIL output. The CME related input parameters for cone models are generally found through geometrical considerations of Large Angle and Spectrometric Coronagraph on board the Solar and Heliospheric Observatory (SOHO/LASCO) [*Brueckner et al.*, 1995] images from the C3 telescope (described by *Xie et al.* [2004]) and are used for simulations in a number of papers [*Taktakishvili et al.*, 2009; *Falkenberg et al.*, 2010; *Vršnak et al.*, 2010]. However, this method potentially suffers from projection effects [*Vršnak et al.*, 2007] and is more efficient in some cases than others. Generally fast and massive CMEs are related to intense flares [*Yashiro et al.*, 2006; *Vršnak et al.*, 2007], so when investigating events of this type, it is an open question whether the flare location can provide a better estimate of the general direction of the CME than analysis of SOHO/LASCO data. However, finding an accurate estimate of the initial direction of the CME may not be sufficient for ensuring that propagation models are successful. Recently, STEREO observations have shown that ICMEs may be deflected latitudinally, instead of just propagating radially [*Kilpua et al.*, 2009; *Liu et al.*, 2010; *Pomoell et al.*, 2010; *Byrne et al.*, 2010], confirming the results of earlier studies [*Wei and Dryer*, 1991; *Filippov et al.*, 2001; *Cremades et al.*, 2006]. Longitudinal deflections on the order of 30° were also found by *Wang et al.* [2004, 2006] and *Shen et al.* [2009], where fast ICMEs tend to be deflected eastward with the IMF Parker spiral and slower ICMEs are deflected against the IMF Parker spiral.

[5] Most of the studies mentioned above dealt with measurements made at heliocentric distances of 1 AU or less. Studies of solar events at distances greater than 1 AU should provide important additional constraints on the propagation and evolution of events. There have been relatively few such studies to date, though spacecraft capable of detecting ICMEs and SEPs have been at Mars continuously since 1997. Two studies relevant to propagation of large events to the orbit of Mars were performed by *Futaana et al.* [2008] and *McKenna-Lawlor et al.* [2008], using both Venus Express, Mars Express and data from the near Earth environment (SOHO and Geostationary Operational Environmental Satellite (GOES)) to study large events in December 2006. *Futaana et al.* [2008] reported increased atmospheric plasma escape at both Venus and Mars, while noting that increased ion escape during large events has previously been measured at Earth [*Cully et al.*, 2003]. They also noted that both ICMEs and SEPs may span more than 90° at 1 AU, as supported by *Reames* [1999] where the ICME shock is seen to span 110° in heliocentric longitude at 1 AU. *McKenna-Lawlor et al.* [2008] modeled the events using the HAFv.2 model and found good correspondence for arrival time at Earth and at Mars; while only weak to reasonable correspondence at Venus. Mars Global Surveyor (MGS) Magnetometer (MAG) and Electron Reflectometer (ER) data has also previously been used to study the Halloween 2003 storm period [*Crider et al.*, 2005; *Espley et al.*, 2005], indicating that the Martian magnetosphere was compressed and that plasma outflow was increased; these studies did not deal with propagation, which is the focus of the effort presented here.

[6] In the present study we focus on simulation of fundamental ICME propagation parameters such as arrival time and signal amplitude of in situ measurements. We apply the CCMC, slightly simplified version, of ENLILv2.6, which is a modern state-of-the-art 3-D MHD time-dependent code, to two events: a 17 November CME and associated flare, and two CMEs on 22 November with associated flares. For these events we use two methods of finding input parameters for the model, both based on analysis of SOHO/LASCO images, and validate these against data from both Earth and Mars. We then evaluate the multipoint observations of Earth and Mars data to see if the input parameters for the simulations can be improved based on the knowledge obtained from multipoint observations. We also investigate the usefulness of MGS data studying both ICMEs and SEPs, as the MGS instruments were never meant to study these phenomena.

2. Data

[7] The data we use for determining the arrival time of the ICMEs at Earth is plasma and magnetic field data from the OMNI database (generously provided and maintained by Goddard Space Flight Center's National Space Science Data Center), in this case composed of data from the Advanced Composition Explorer (ACE), Geotail and WIND satellites shifted to the nose of the Earth's bow shock (first and second panels of Figure 1). For energetic particle data at Earth we use 5 minute corrected in situ data from GOES 8 (third panel in Figure 1).

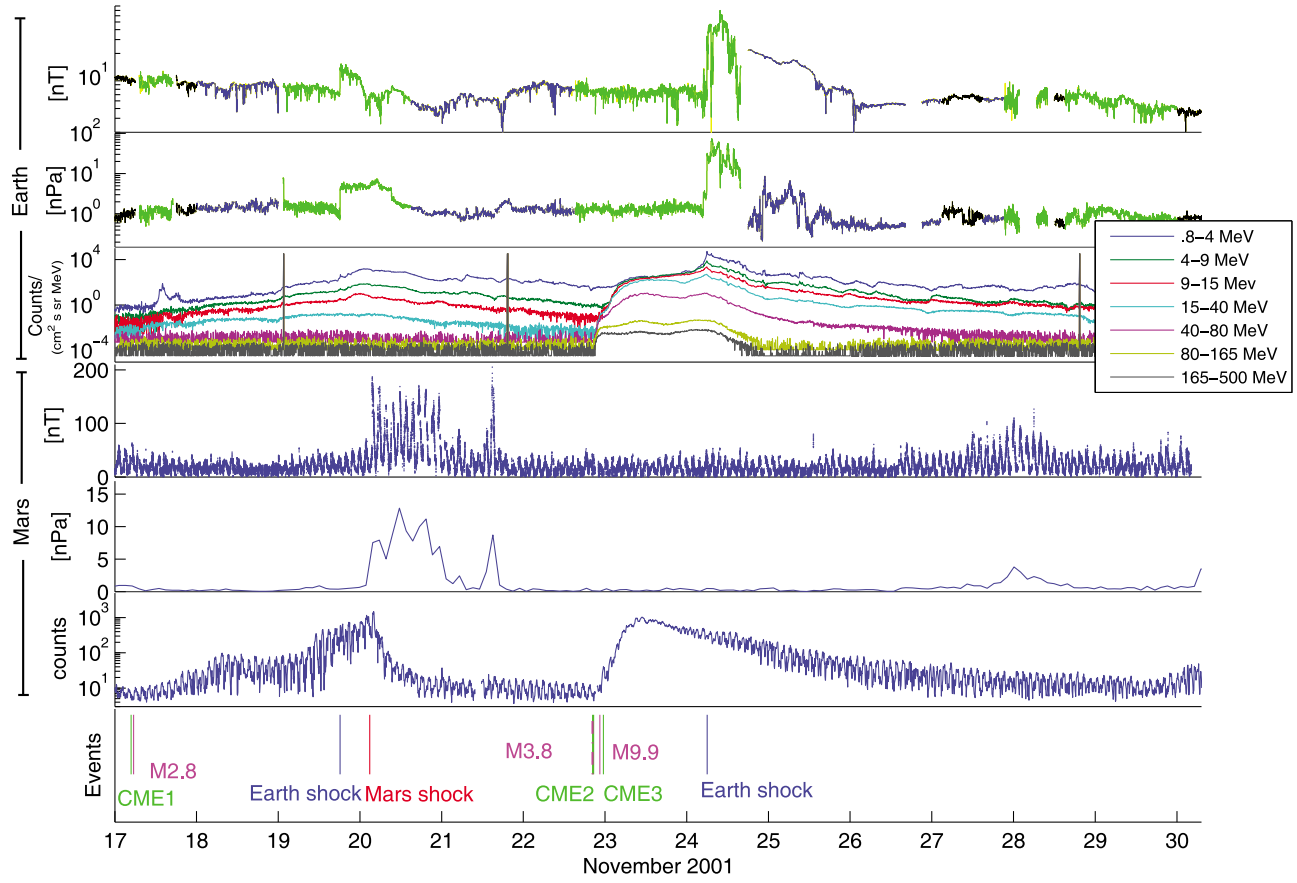

Figure 1. Observations from Earth and Mars for a series of CME and flare events in November 2001. The last panel shows timing of events from Table 1 and shock arrival at both planets. First and second panels show OMNI data (Geotail in Green, ACE in blue, WIND in black) from the nose of Earth's bow shock, magnetic field intensity and dynamic pressure, respectively, both on semilogarithmic scales. The third panel shows particle data from GOES 8 with energies shown in the legend at the right; the seeming vertical lines are spurious data points and should be ignored. The fourth panel shows magnetic field intensity measurements from MGS, when the remnant crustal field according to the Cain model [*Cain et al.*, 2003] is less than 10 nT. The fifth panel shows the proxy for upstream dynamic pressure at Mars. The sixth panel shows the count rates from the highest energy channel of the ER (18 keV) where evidence of penetrating particles (>30 MeV) is seen. The last panel shows the timeline of important events; CME appearances in SOHO/LASCO C2 (green), flare launches from the Sun (purple), shock arrivals at Earth (blue), and shock arrivals at Mars (red).

[8] For Mars we use observations from the MGS magnetometer (MAG) and Electron Reflectometer (ER). The MGS MAG instrument provided vector magnetic field measurements accurate to ~1 nT at a worst case time resolution of 3 seconds. MGS also carried the ER instrument which was designed to measure electron populations in the 10 eV to 20 keV range, but also provided fortuitous measurements of high energy particles which penetrated the instrument, giving rise to elevated count rates simultaneously in all energy channels. The ER data, especially when combined with the MAG data, give new information on the effects of SEP and ICME events on Mars over ~2/3 of a solar cycle.

[9] MGS orbited Mars in a Sun-synchronous mapping orbit at ~400 km altitude from 1999 to 2006, providing data over a very long time period, including the last solar maximum in 2000/2001 when solar activity was high. During this period MGS orbited within Mars' induced magnetosphere, so that the observations were not recorded in the upstream solar wind at 1.5 AU by MGS during this period. MGS had no instruments measuring ion properties (i.e., speed, density etc.), meaning that even when MGS was in its elliptical aerobraking phase (1997–1999) and therefore spent at least part of its orbit in the pure solar wind, there was no way of measuring solar wind moments.

[10] We use a proxy for upstream solar wind pressure at Mars (Figure 1, bottom) derived from MGS data [*Brain et al.*, 2005]. The MGS pressure proxy data are calculated from an estimate of the magnetic field intensity at the subsolar point in the Martian magnetosphere, as measured by MGS. The MGS pressure proxy is then converted from magnetic field intensity (B) to pressure (P_{mag}) by using $P_{mag} = \frac{B^2}{2\mu_0}$ (where μ_0 is the vacuum permeability given by $4\pi \cdot 10^{-7}$). This pressure is assumed to be comparable to the pressure of the upstream solar wind [*Vennerstrom et al.*,

2003; *Crider et al.*, 2003, 2005; *Brain*, 2006; *Dubinin et al.*, 2008], which is typically dominated by the dynamic pressure. The dynamic pressure of the solar wind is then estimated using the formula described by *Zhang et al.* [1991], *Vennerstrom et al.* [2003],and *Crider et al.* [2003] of $P_{mag} \simeq K \cdot P_{dyn}$ where $K = 0.88$; we disregard a term including the solar zenith angle as this is already incorporated in the estimate of the magnetic intensity at the subsolar point. The magnetic intensity at the subsolar point (and therefore the pressure proxy) is calculated once per orbit of MGS around Mars, meaning that the pressure proxy has a cadence of about 2 h.

[11] The pressure proxy relies on the assumption that the pressure at MGS orbital altitude (400 km) is dominated by magnetic pressure. This is true when MGS is in the magnetic pileup region of Mars, i.e., below the MPB (Magnetic Pileup Boundary). During times when the plasma region is compressed (i.e., during an ICME) that assumption is not necessarily valid as MGS may be above the MPB and therefore in the magnetosheath region of Mars [*Crider et al.*, 2005; *Espley et al.*, 2005; *Brain et al.*, 2005], where thermal pressure is nonnegligible. In times of ICMEs, thermal pressure in the solar wind may also be nonnegligible, and as ICMEs carry large magnetic clouds, the magnetic pressure in the solar wind is also nonnegligible, meaning that the solar wind pressure is also not necessarily dominated by its dynamic pressure. The magnetic cloud of an ICME may also cross the bow shock and increase the magnetic pressure measured by MGS. The assumption of $P_{dyn}^{SW} = \frac{P_{mag}^{MGS}}{K}$ (where P_{dyn} is the dynamic pressure in the solar wind and P_{mag}^{MGS} is the magnetic pressure measured by MGS) is therefore a rough assumption, and should be treated carefully. However, it is currently our best method of estimating the characteristics of ICMEs at Mars prior to the arrival of Mars Express at Mars in December 2003.

[12] The particle data we use for Mars is ER data from the three highest energy electron channels, i.e., ~11 keV, 14 keV and 18 keV [*Brain*, 2006, D. A. Brain et al., MGS measurements of solar storms and their effects, submitted to *IAA Study of Radiation From the Sun to Mars*, 2010]. The instrument itself can be penetrated by particles with an energy larger than ~30 MeV (for protons) which then hit the micro channel plate of the ER instrument and are ultimately recorded as counts. These particles will therefore cause abnormally large count rates in all energy channels, but their signature is most obvious in the highest energy channels (10–20 keV), as very few high energy suprathermal electrons are typically present. At times when the signal from penetrating particles dominates the signal from suprathermal electrons, the counts in the three highest energy channels should be nearly identical since the flux of penetrating particles striking the microchannel plate is not influenced by the energy that the instrument is tuned to. At times when suprathermal electrons dominate the signal, the count rate should decrease with energy, due to the suprathermal electron energy distribution. At quiet times the signal in these three channels is dominated by galactic cosmic rays (GCRs), but at times of solar events, SEPs are clearly evident. However, it is difficult to distinguish the counts caused by suprathermal electrons from those caused by high energy penetrating protons. A similar method is used to detect particles on the Mars and Venus Express missions [*Futaana et al.*, 2008; *McKenna-Lawlor et al.*, 2008].

3. 17 November 2001 Event

[13] During late November 2001, Earth and Mars were separated by 56 degrees in solar longitude, as shown in Figure 2. Mars trailed Earth, so that the two planets occupied interplanetary magnetic field lines separated by only 20–25 degrees at the Sun, assuming a Parker spiral magnetic field configuration (the ideal Parker spiral connection at 400 km s^{-1} is given when Mars trails Earth by ~33 degrees).

[14] On 17 November at 05:30:06 UT the SOHO/LASCO C2 coronagraph observed a halo CME with initial speed of 1379 km s^{-1}. The ensuing ICME was observed at both Earth and Mars, and is hereafter referred to as CME1/ICME1. Initial parameters for CME1 and its associated flare are listed in Table 1.

[15] ICME1 was measured by the Geotail satellite at the nose of Earth's bow shock on the 19th at 18:43 UT and by MGS at Mars about 8 h later, as seen in Figure 1. The ICME is identified at Earth by its leading shock, marked by a sharp increase in speed, density, temperature and magnetic field intensity, and at Mars as a sharp increase in magnetic field intensity, reflected in the pressure proxy. At Mars a shock signature in the ER data, characterized by a sudden sharp increase in background count rate at 02:52 UT on the 20th, is also used to identify the ICME shock arrival.

[16] The fact that the ICME is clearly visible at both Earth and Mars means either that the ICME front spanned a longitude range that encompassed both planets, or that the ICME propagated very nonradially. The relatively small difference in arrival time of the ICME at the two planets (~8 h) indicates either that the ICME propagated at high speed ($\gtrsim$2000 km s^{-1} between 1AU and 1.5 AU compared to a typical propagation speed of ICMEs at this solar distance of <1000 km s^{-1}), or that the curved ICME shock front encountered Mars square on and only grazed Earth. We favor the latter interpretation as the more likely option. In this case Mars would have been 'hit' relatively earlier than Earth, and also with a relatively larger dynamic pressure. The dynamic pressure measured near-Earth has a maximum of 7.5 nPa while the pressure proxy at the subsolar point at 400 km at Mars has a maximum on the order of 13 nPa (Figure 1).

[17] In Table 2 some propagation parameters for CME1 extracted from SOHO/LASCO images are provided (this is described in more detail in section 5). The direction of CME1 inferred from these parameters is indicated in Figure 2. Three different propagation scenarios for CME1 are plotted in Figure 2. In all scenarios it is clear that CME1 propagated in a direction intermediate between the positions of Earth and Mars.

[18] The exact relationship between CMEs and flares is still an open question, however, substantial evidence that the two phenomena are related, at least for larger flares (M and X classes) has been provided by *Yashiro et al.* [2006]. Correlation between the total flare energy and the kinetic energy of the CME is also found [*Emslie et al.*, 2005; *Dennis et al.*, 2006]. For CME-related and accelerated SEPs, the particles mainly arrive with the ICME shock front, however, particles arriving both before and after may still be flare related. For

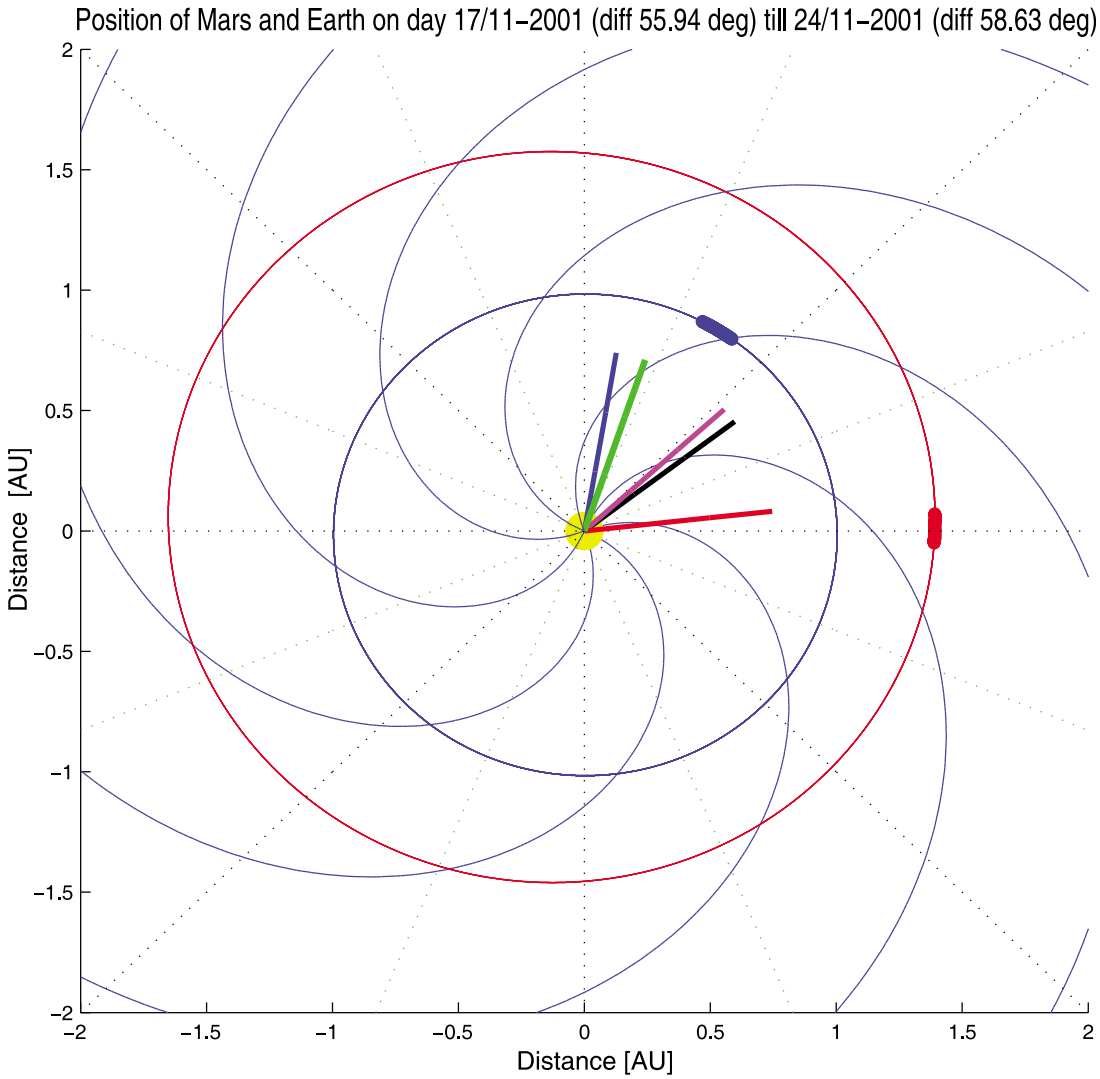

Figure 2. Position of Earth (blue dot) and Mars (red dot) on 17 and 24 November 2001 with a nominal Parker spiral at 400 km s^{-1} (blue lines). The direction of the CMEs simulated with ENLILv2.6 (shown in Figures 4 and 6) are shown as colored straight lines protruding from the Sun. For CME1 lines are black (first run), purple (second run) and red (third run). The direction of CME2 and 3 are shown in blue and green, respectively.

this reason we chose to take the flares related to the CMEs into consideration when looking at the SEP events for both Earth and Mars.

[19] About 45 min before CME1 first appeared in SOHO/LASCO C2, a M2.8 flare was launched from S13E42 (latitude/longitude location on the Sun), active region (AR) 9704 at 04:49 UT (Table 1). The flare occurred at E42, and Earth is typically connected to solar longitude W58, ~100° to the west. At this time an ideal Parker spiral at 400 km s^{-1} connects Mars to ~W33, about 25° closer to the flare

Table 1. CME Events in Late November 2001 and Related Flares[a]

	CME; SOHO/LASCO				Flare; GOES X-ray			
	Start Time (UT)	Initial Speed (km s^{-1})	Speed at 20 R_S (km s^{-1})	Halo	Start Time (UT)	Class	Location	Active Region (NOAA)
CME1	17th 05:30:06	1379	1350	Halo (OA)	17th 04:49:00	M2.8	S13E42	9704
CME2	22nd 20:30:33	1443	1307	Halo (OA)	22nd 20:18:00	M3.8	S25W67	9698
CME3	22nd 23:30:05	1437	1409	Halo (BA)	22nd 22:32:00	M9.9	W36[b]	9704

[a]The CME parameters listed here are those listed in the SOHO/LASCO catalogue. The start time is the first appearance in LASCO C2. All three CMEs were Halo CMEs displaying asymmetries. OA stands for Outline Asymmetry and BA for BrightnessAsymmetry. The flare parameters are from the GOES X-ray catalogue. During this time, using an ideal Parker spiral at 400 km s^{-1}, Earth is magnetically connected to ~W58 and Mars to ~W33.
[b]The location is estimated from the location of an earlier flare from the same active region.

Table 2. CME Cone Input Parameters for CMEs 1, 2, and 3 Extracted Using the XOL Method [*Xie et al.*, 2004][a]

Parameter	XOL by Eye	Automated Conic CME Analysis Tool	Modified Parameters
	CME1		
CME start date	17 November 2001	17 November 2001	17 November 2001
CME start time	06:42 UT	08:08 UT	06:42 UT
Latitude	10°	10°	10°
Longitude	−19°	−14°	−50°
Radius	31°	34°	40°
CME speed	844 km s^{-1}	1142 km s^{-1}	1200 km s^{-1}
	CME2		
CME start date	22 November 2001	22 November 2001	-
CME start time	22:52 UT	23:05 UT	-
Latitude	−14°	−10°	-
Longitude	18°	24°	-
Radius	35°	28°	-
CME speed	1459 km s^{-1}	1312 km s^{-1}	-
	CME3		
CME start date	23 November 2001	23 November 2001	-
CME start time	1:10 UT	02:07 UT	-
Latitude	15°	4°	-
Longitude	38°	15°	-
Radius	71°	42°	-
CME speed	2809 km s^{-1}	1159 km s^{-1}	-

[a]Parameters extracted using the XOL method by eye (left column, result shown as black line in Figure 4 for CME1), automated (middle column, result shown as purple line in Figure 4 for CME1 and in Figure 6 for CME2 and 3) and the modified parameters (right column, result shown as red line in Figure 4 for CME1). Parameters for CME2 and 3 were not modified. The remaining input parameters in ENLILv2.6 were fast solar wind speed limit, 625 km s^{-1}; fast solar wind density scaling factor, 300 cc; maximum solar wind temperature, 0.8 million K; cloud density, 1200 cc; cloud temperature, 4 million K for CME1 and 0.8 million K for CME2 and 3; elongation factor, 1 and a spherical cloud (see *Falkenberg et al.* [2010] for an extensive description of these and their influence on the ENLIL output). All runs were done with a resolution of 256 × 60 × 180, using WSA version 1.6 input and Mount Wilson Observatory magnetograms.

location than the connection to Earth. However, neither planet is very well connected to the origin of the flare. The Parker spiral connection, however, is not necessarily valid in times of disturbed solar wind, and SEPs are also believed to be produced in the shock front of the ICME, therefore magnetic connection to the flare origin is not a prerequisite to detect SEPs [*Klein et al.*, 1999].

[20] The measurements of SEPs arriving at Earth and Mars following this flare both show a gradual increase in particle count until the arrival of the ICME shock, and then a sharp decrease at Mars and a slow decrease at Earth (Figure 1). Both of these SEP profiles should be classified as gradual events [*Reames*, 1999], where the predominant acceleration of the SEPs is by the ICME shock front. However, the flare is significant enough to cause substantial SEPs with or without an ICME, and the SEPs at both planets are detectable more than two days before the ICME shock arrival, so it seems that at least some of these particles are flare related. At Mars this is one of the 15 largest SEP events recorded by MGS, i.e., in the period 1999–2006. Only 10 SEP events are associated with higher background count rates in the MGS ER data. We must be cautious to note that background count rates can be comprised of both SEPs and 10–20 keV electron fluxes, as outlined in section 2. However SEPs by themselves likely contribute to at least an order of magnitude increase in the count rates for this event. At Earth the SEP event is almost unnoticeable when only looking at particles above 30 MeV (the ER instrument is only penetrated by particles above ~30 MeV). This discrepancy in the seeming magnitude of the SEP event at the two planets could be caused by two things. First of all, only the flank of the ICME seems to have hit Earth (as described above and section 5). Second, assuming the flare itself did contribute to the SEP signal at Earth and Mars, the better magnetic connection to Mars may play a role. Both effects would cause Mars to receive the highest relative flux of high energy particles, as seen in the data (Figure 1).

4. 22 November 2001 Event

[21] Following CME1, two halo CMEs were launched from the sun on 22 November with first appearances in SOHO/LASCO C2 at 20:30 and 23:30 UT, both with velocities of ~1400 km s^{-1}, hereon referred to as CME2 and 3 respectively (Table 1). Smaller halo CMEs were also launched between 17 and 22 November, however, these are disregarded in this study as they are minor CMEs and no unambiguous response is seen at either Earth or Mars in response to them.

[22] An ICME caused by either CME2 and 3 which have merged, or only one of the two, is evident in measurements made near Earth on 24 November (Figure 1) with a much higher amplitude signal in all parameters than ICME1. ICME2 and 3, however, are not apparent in the Mars data. Some small scale pressure features are seen as late as 28 and 30 November, but these are too small and too late to be plausibly associated with CME2 and 3, and simulation of the events (section 5) suggests that these features are associated with Mars passing through the heliospheric current sheet. If the feature on 28 November at Mars was to be associated with these CMEs, the average propagation speed from the Sun would be around 500 km s^{-1} while the average propagation speed from the Sun to Earth was almost 1300 km s^{-1}. Several other phenomena could also be responsible for these features at Mars such as smaller CMEs or high speed streams. The ICMEs therefore seem to have largely missed Mars, even though the longitudinal distance between the two planets was still less than 60° at the time.

[23] In Table 2 the propagation parameters for CME2 and 3 extracted from SOHO/LASCO images are shown (described in more detail in section 5), and their initial propagation directions are indicated in Figure 2. Both CMEs were directed ahead of Earth while Mars was trailing, contrary to CME1, explaining why they were not seen at Mars.

[24] The flares related to CME2 and 3 are identified as the M3.8 flare, launched from S25W67, AR 9698 at 20:18 UT and M9.9 from AR 9704 (location not listed in the GOES X-ray catalogue) at 22:32 UT on 22 November (Table 1). Smaller flares were also launched around this time, but we choose to focus on the most prominent flares for this study. One of the smaller flares (M1.2 at 17:00 UT from S18W33 AR 9704) originates from the same active region as the M9.9 flare (associated to CME3), which allows us to estimate the longitudinal location of this flare to be around W36 as the active region would have moved slightly west in the 6 h between the two flares. The latitude of the flare is less

important for our purpose here, but it may also have changed in the time between the two flares, and the active region itself probably spans a few degrees in both latitude and longitude, giving rise to some uncertainty in the location estimate.

[25] The M9.9 flare (associated to CME3), estimated to have originated from ~W36, would have been better magnetically connected to Earth than the flare related to CME1, but almost ideally connected to Mars. Earth is typically best connected to W58. At this time Mars is trailing Earth by ~56 degrees in heliocentric longitude, which means that Mars would be connected to ~W33 using a nominal Parker spiral at 400 km s^{-1}. The M3.8 flare (associated to CME2) originated from W67 and was therefore rather well connected to Earth, but significantly less so to Mars. The assumption of a nominal Parker spiral at 400 km s^{-1} seems to be supported by observations.

[26] Following these flares we see a sharp increase in particles at Earth, with the highest energy particles arriving first, followed by a gradual increase of particles over a little more than half a day before a slow gradual decrease starts in the high energy particles, interrupted by the ICME shock arrival where a small peak in particle flux is observed (particularly at low energies), and the particle rates slowly decrease towards background levels again. At Mars we observe a relatively fast gradual increase in particles (half a day) followed by a very slow gradual decrease. However, no shock arrival is evident in either the ER or in MAG data, and the ICME shock front is assumed to have missed Mars completely (Figure 1). As no shock arrives at Mars, the event at Mars must be classified as an impulsive event [*Reames*, 1999], where the particles are accelerated by the flare itself only. The reason for the presence of shock accelerated particles at Earth and not at Mars in connection with the 22 November CMEs/flares is that no shock arrived at Mars. The SEP signal lasts several days at Mars, which is not unusual and is assumably due to the scattering of the particles throughout interplanetary space.

[27] Looking more closely at the earliest part of the SEP events at both planets (Figure 3), we see that the first SEPs arrive at Earth at 21:30 UT on 22 November. These are necessarily unrelated to the M9.9 flare as this was launched at 22:32 UT, and must therefore be from the M3.8 flare at 20:18 UT. At Earth we then see an additional increase in particle flux around 00:30 UT on 23 November which seems to be the effects of the M9.9 flare. At Mars the SEPs start arriving predominantly around 23:30 UT on 22 November and no indications of two SEP events are obvious. The timing of this signal lines up nicely with the M9.9 flare, which is not only a bigger flare than the M3.8 flare, but also better magnetically connected to Mars. The SEP event on Mars therefore seems to be almost exclusively the effect of the M9.9 flare. This means the M3.8 flare from W67, 34° west of the theoretically ideal magnetic connection to Mars, largely misses Mars, while the signature of the M9.9 flare, 3° west of theoretically ideal connection to Mars and 22° east off theoretically ideal connection to Earth, looks rather similar at the two planets. The SEP profiles related to the M9.9 flare at either planet display a slow gradual increase of about two orders of magnitude (the ER data are uncalibrated and not in physical units, this is therefore only a relative comparison). At both Earth and Mars this is one of the 7 biggest impulsive SEP events in the period between 1999 and 2006, when disregarding shock values at Mars and focussing on high energy particles (>30 MeV) in the GOES data for Earth.

[28] The signal from the M9.9 flare seen at Mars, having particles that arrive at 1.5 AU almost immediately after the flare eruption, together with the absence of a signal from the M3.8 flare, underlines the importance of being magnetically connected to the origin of an event. At Earth the signal is more 'messy' due to the arrival of particles from a previous flare and the ICME shock front, but similarities between the profiles are still seen, confirming the validity of using the MGS ER data to observe SEP events at Mars.

5. MHD Simulation

[29] For this study we simulated possible propagation scenarios for CME1 using ENLILv2.6 which is available for online runs at the Community Coordinated Modeling Center (CCMC) at Goddard Space Flight Center. This is a simplified version of the ENLIL model [*Odstrcil and Pizzo*, 1999; *Odstrcil et al.*, 2004]. ENLIL is a 3-D time-dependent MHD solar wind model, capable of propagating features, representing CMEs, through a realistic model of the solar wind. We use a resolution of 256 × 30 × 90 (resolutions 512 × 60 × 180 and 1024 × 120 × 360 are also available). ENLILv2.6 can be run without a CME or with up to 5 CMEs in one run, which spans one Carrington Rotation. As input for the background solar wind in ENLILv2.6, we use input from the Wang-Sheeley-Arge model [*Arge et al.*, 2004] version 1.6 using Mount Wilson Observatory (MWO) magnetograms. The CCMC version of ENLIL has also previously been verified against data recorded near-Earth [*Falkenberg et al.*, 2010; *Taktakishvili et al.*, 2009; *Lee et al.*, 2009] and does quite well at predicting arrival times and major solar wind parameters near-Earth. To our knowledge it has not been used to reproduce the pressure proxy at Mars, however, this has previously been attempted by *Jackson et al.* [2007] with good results, using the Heliospheric Tomography model also available at CCMC. The HAFv.2+3-D MHD is another option for simulating ICME propagation through a realistic solar wind model [*Intriligator et al.*, 2005; *Wu et al.*, 2007].

[30] To run the ENLILv2.6 model, one only needs input relevant to the CME inserted in the model, as the background solar wind is inferred from the WSAv1.6 model using the MWO magnetograms. The input parameters (see *Falkenberg et al.* [2010] and *Taktakishvili et al.* [2009] for an extensive description of these and their effects on the model) for the CME are those of time, speed, density, temperature, direction and angular width, as ENLILv2.6 does not include a magnetic cloud in the CME. The majority of these inputs (i.e., time, speed, direction and width) can be inferred from SOHO/LASCO images and the procedure described by *Xie et al.* [2004, hereinafter XOL method], which is basically a geometric consideration using consecutive SOHO/LASCO images, in which ellipses are drawn around the CME so that all of the area presumably related to the CME is included in the ellipse, while this is still a perfect ellipse with at least one axis passing through the center of the Sun. The CME is then assumed to propagate in a cone manner and a perfect cone protruding from the Sun is then

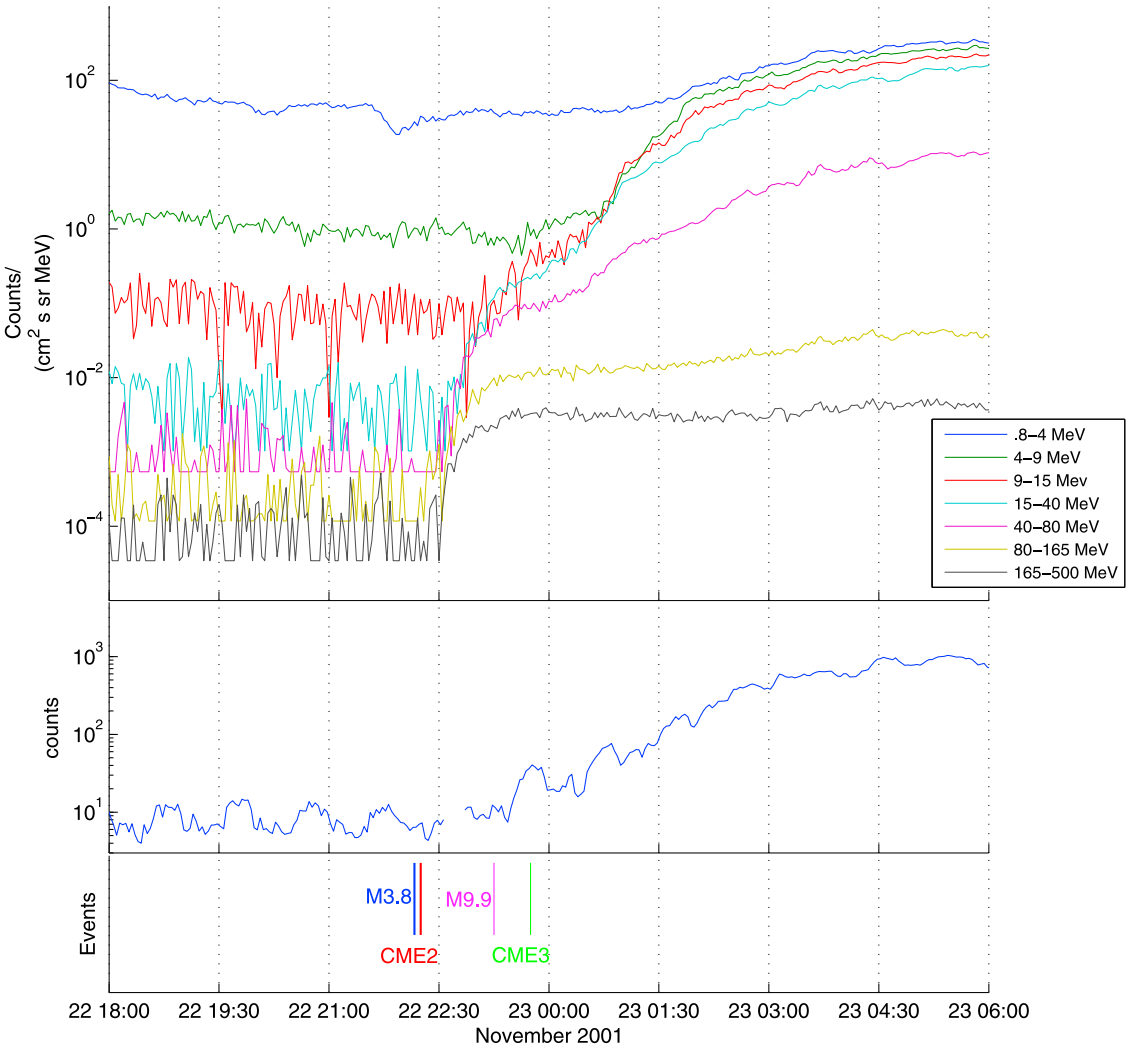

Figure 3. Zoom of Figure 1 showing only the particle data from (top) Earth and (middle) Mars with the (bottom) timeline of the events.

fitted to these ellipses, giving the initial direction, width, speed and time of the CME at the inner boundary of ENLIL at 21.5 solar radii. This method was used by both *Taktakishvili et al.* [2009] and *Falkenberg et al.* [2010] and is one of the only methods of obtaining realistic input parameters for ENLIL before the era of the STEREO spacecraft. Typically the XOL method is implemented by hand, but recently an automated tool using the method has been developed at CCMC [*Pulkkinen et al.*, 2009]. The automated tool has two main advantages: First, the image analysis is done digitally and is therefore not dependent on subjective estimates, nor one's ability to accurately draw ellipses around the CME, also this means that the automated method uses the actual cross-sectional area of the CME rather than an ellipse approximating the outline; Secondly, the automated tool also provides an estimate of the error bars on the determination of the parameters.

[31] Following the XOL procedure for cone model parameter extraction, the parameters obtained for input at the inner boundary of ENLIL (at approx. 21.5 solar radii) are shown in Table 2. Values obtained using the XOL method both by hand and using the automated tool are shown in Table 2. Here we use the notation of the newly updated ENLILv2.6 interface of the CCMC Web page, where latitude and longitude 0° are toward Earth. Using the ENLILv2.6 model one should be aware that the model does not incorporate a magnetic cloud in the CME, so the magnetic signal arriving with the ICME is only a consequence of compression in the shock front of the ICME. ENLILv2.6 will therefore tend to underestimate the magnetic field intensity and overestimate the density in ICMEs, as ICMEs in ENLILv2.6 are dominated by dynamic pressure [*Taktakishvili et al.*, 2009; *Falkenberg et al.*, 2010].

[32] Using the parameters from the left column of Table 2 one sees a clear discrepancy between the satellite data and the model (see black line in Figure 4). The modeled event at Earth looks plausible both with regards to signal strength and arrival time, though arriving ~9 h too early. See the top row of Table 3 for a numerical presentation of the performance. At Mars (black line in Figure 4 (bottom), however, the modeled event arrives nearly 1.5 days late, with a vastly underestimated amplitude (see Table 3). If one takes a closer look at the path of the ICME in interplanetary space (a snapshot of which is seen in Figure 5 (top)) one clearly

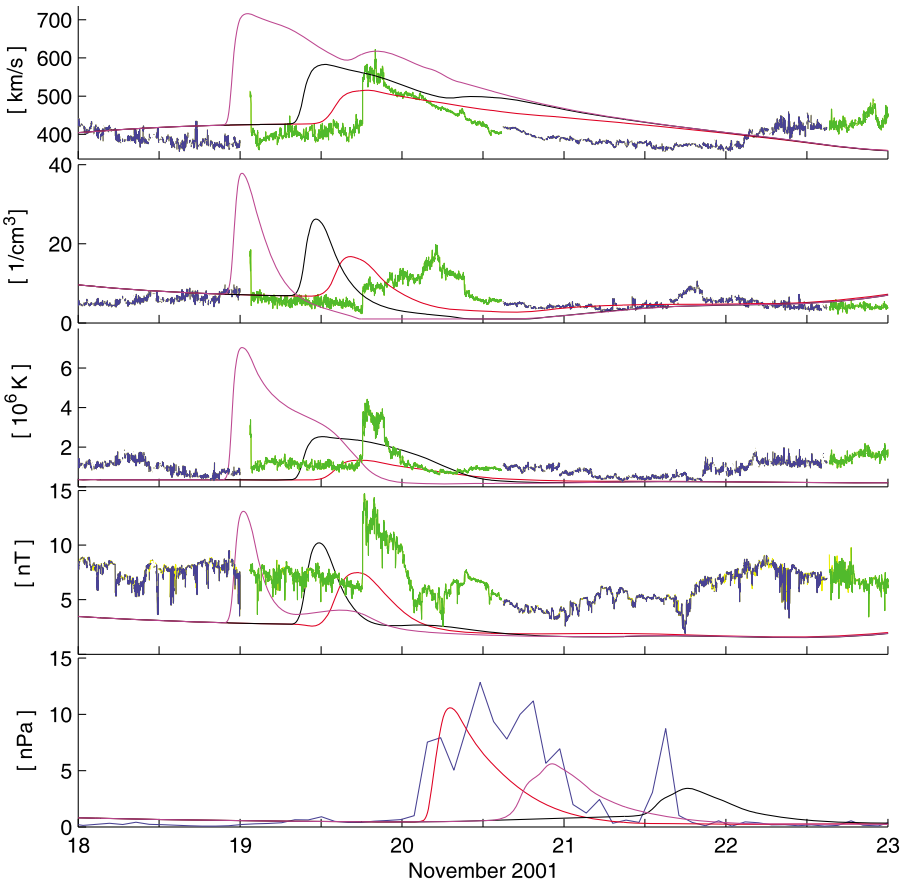

Figure 4. ENLILv2.6 simulations of CME1. Panels from top show speed, density, temperature and magnetic field intensity at the nose of Earth's bow shock, and dynamic pressure at Mars. For the top four panels, Geotail data shown in green, and ACE data are shown in blue. The last panel shows the MGS pressure proxy in blue. ENLILv2.6 simulation shown in black (first run, XOL method by eye), purple (second run, automated conic CME analysis tool), and red (third run, modified parameters). Input parameters used for the ENLILv2.6 runs are those listed in Table 2 for CME1 in the left, middle, and right columns corresponding to the first, second, and third runs, respectively.

sees that while the event hits Earth fairly square on it only grazes Mars, therefore arriving not only late but with an amplitude that is much too low, compared to that expected from the MGS pressure proxy. Since we know ICME1 encountered Mars within 3 days of its launch from the Sun, it is also obvious that the speed in the left column of Table 2 is much too low.

[33] Using the parameters found from the automated XOL method (middle column in Table 2, result seen in purple in Figure 4), the signal arrives 19 h early near-Earth, with overestimated amplitude in almost all parameters (see middle row of Table 3 for a numerical presentation of the performance). The signal at Mars arrives 14.5 h early and with about half the pressure of the pressure proxy. These rather significant changes from the first run are primarily due to the higher initial speed.

[34] Looking at the results of both of these runs it seems that a modification of the input parameters is needed in

Table 3. Performance of ENLILv2.6 for Parameters Listed in Table 2 for CME1[a]

	Near-Earth					Mars	
	Arrival Time	Speed	Density	Temperature	Magnetic Field Strength	Arrival Time	Dynamic Pressure
XOL by eye	−9 h	0%	20%	−37%	−33%	36 h	−65%
Automated conic	−19 h	21%	100%	75%	−13%	14.5 h	−50%
Modified	−5 h	−9%	0%	−75%	−50%	1.5 h	−13%

[a]The arrival time is listed as the difference in arrival time in hours, where negative indicates arrival before the satellite data and positive arrival time after the satellite data. The speed, density, temperature, and magnetic field strength at the nose of Earth's bow shock and the dynamic pressure at Mars are listed as the deviation of the maximum value of these from the maximum value measured by satellites. The arrival times and maximum values for both data and model are readfrom the plots using zoom.

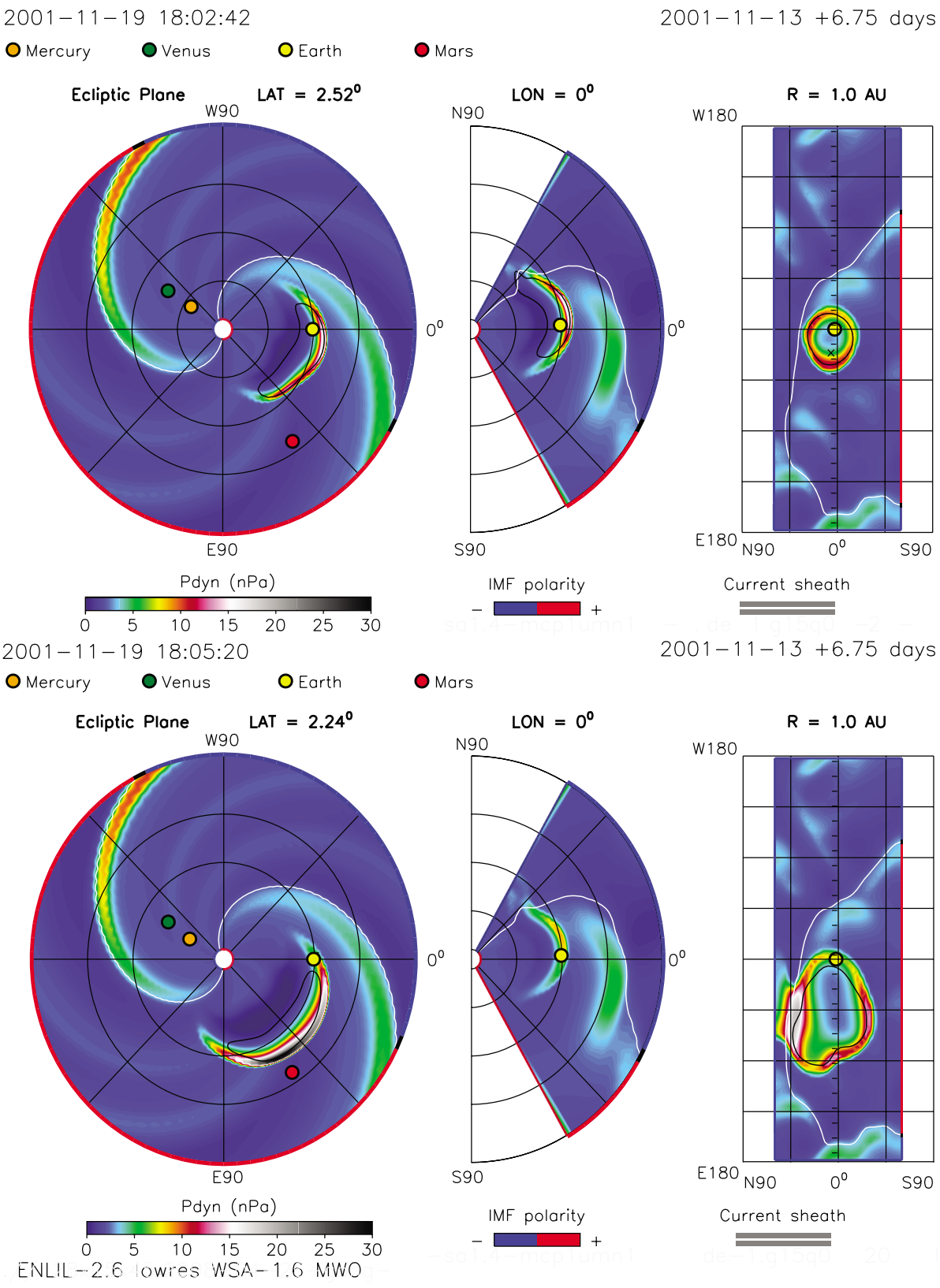

Figure 5. Snapshot of ENLILv2.6 runs for CME1. (top) First run and (bottom) third run. Dots show the position of Earth (yellow), Mars (red), Mercury (orange), and Venus (green). White lines show sector separations in the solar wind, and red and blue lines surrounding the plots show the IMF polarity. Input parameters used for the ENLIL runs are those listed in Table 2 for CME1 in the left and right columns corresponding to the first and third runs, respectively.

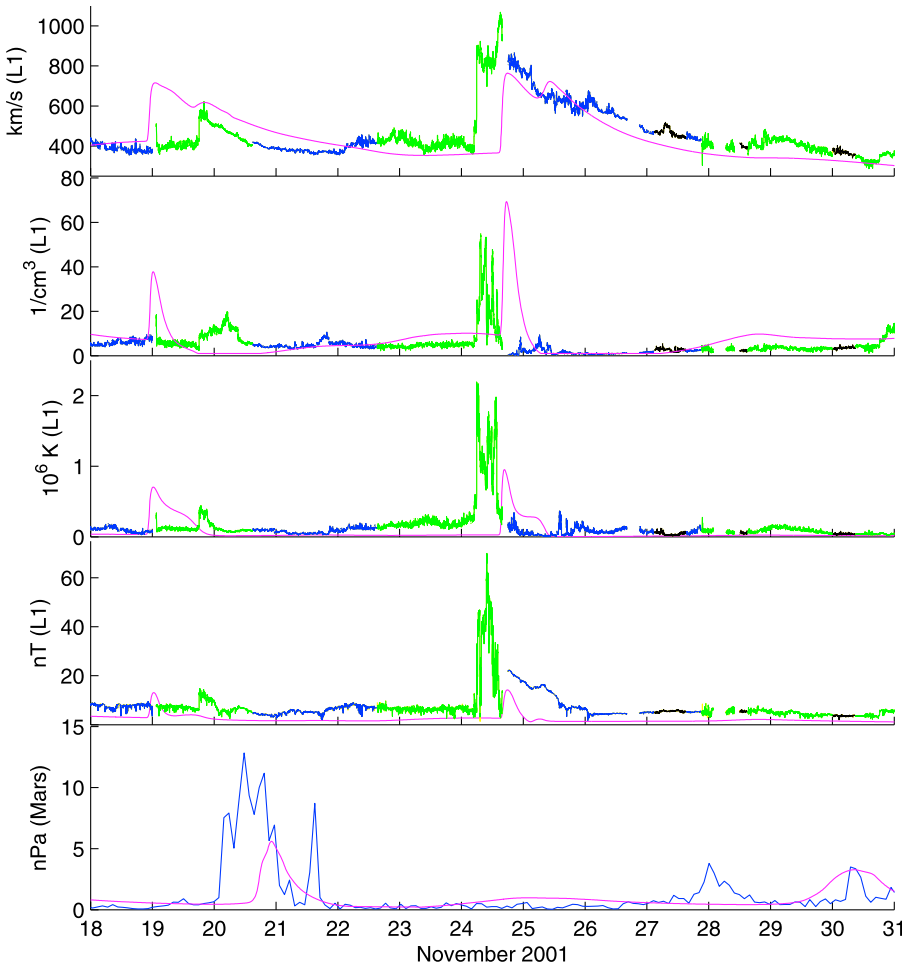

Figure 6. ENLILv2.6 simulation of 17 November CME and the two 22 November CMEs. Panels from top show speed, density, temperature and magnetic field intensity at the nose of Earth's bow shock, and dynamic pressure at Mars. For the top four panels, Geotail data shown in green, and ACE data are shown in blue. The last panel shows MGS pressure proxy in blue. ENLILv2.6 simulation including all three CMEs is shown in purple (second run, automated conic CME analysis tool). Input parameters used for the ENLIL runs are those listed in the middle column of Table 2 for all three CMEs.

order to get an ENLILv2.6 run better resembling the data at both planets: Considering the measured 8 h time difference in arrival between Earth's bow shock and Mars, we chose a speed of 1200 km s^{-1} at 21.5 solar radii, which is slightly lower than that listed for 20 solar radii in the SOHO/LASCO catalogue (1350 km s^{-1}) and slightly higher than what was found by the automated XOL method (1142 km s^{-1}). A difference in initial speed of the CME of less than 50 km s^{-1} is not a significant change, but it is noticeable. We then modified the longitudinal direction and the width of the CME to hit Mars and only graze Earth (see modified parameters in right column of Table 2), in order to correspond to our interpretation of the observations. The modification of the longitudinal direction of the CME builds on a simple trial and error method, having performed 34 different runs (not included here) where mainly direction, but also speed and width were changed. It serves only as a caution to incorporate the results of interpretation of multipoint satellite data when determining how an ICME must have propagated, instead of relying solely on the input parameters found by the XOL method. The longitudinal direction of the modeled CME is shown in Figure 2 for the three model scenarios presented here. The modified direction of the CME corresponds better with the location of the presumably related M2.8 flare originating from E42 (the modified direction corresponds to E50). This supports the findings of *Temmer et al.* [2009], who reported that the flare position is a good proxy of the CME source location and therefore also direction if radial propagation is assumed. The results of these modifications to the input parameters are seen in Figure 4, and a snapshot of the path of the ICME in interplanetary space is seen in Figure 5 (bottom). Here we see that the ICME does in fact hit Mars square on and only flanks Earth, as desired. In Figure 4 we also see that the ICME arrives less than 5 h early near-Earth, with rather well estimated magnitude of all parameters, with the exception of temperature and magnetic field, which are generally problematic (see bottom row of Table 3). At Mars the dynamic pressure proxy is recreated almost perfectly, with the exception of the pressure peak late on 21 November, which

seems to be caused by either a transient feature of the trailing part of the ICME or some phenomenon unrelated to the events being studied here.

[35] A simulation using the XOL method parameters extracted using the automated tool at CCMC for all three CMEs is shown in Figure 6. This simulation shows that though CME1 is reproduced poorly at Earth using the parameters found with the automated tool, CME2 and 3 are produced rather well. ICME2 and 3 are merged rather quickly in the simulation, which one also would expect, as the later CME is slightly faster according to the SOHO/LASCO catalogue, and the later ICME would also have experienced much less drag traveling in the wake of the ICME in front of it [*Vršnak and Gopalswamy*, 2002; *Vršnak et al.*, 2010], rather than the slower background solar wind. It could also be that only one of the ICMEs did in fact hit Earth instead of the two ICMEs merging, especially considering the very western longitude of the flare related to CME3 (Table 1). This can not be determined from the data or the simulation; one can only deduce that the ICMEs merged in the simulation and hit Earth while neither hit Mars, and the results fit very well with data from both Earth and Mars.

[36] The simulation of all three CMEs show some evidence that the small features seen in the Mars pressure proxy on 28 and 30 November could be due to the crossing of the heliospheric current sheet as Mars crosses this on 30 November in ENLILv2.6 when using input from the WSAv1.6 model with MWO magnetogram.

6. Discussion

[37] The 17 November 2001 CME event provides an opportunity to study an ICME event in a multipoint fashion. This approach suggests that, though the event was classified as a halo event, the bulk of the event missed Earth and hit Mars instead, trailing ~56 degrees behind Earth at the time. This means the ICME must have spanned around 110° in longitude at 1 AU, in correspondence with the findings of *Futaana et al.* [2008] and *Reames* [1999]. In this case modeling enabled us to estimate a more plausible set of input parameters, using the constraints of having arrival time and approximate signal amplitude at both Earth and Mars in a given configuration. Using only data at Earth the ICME looks to be a slower, less significant ICME, which is easily modeled and looks plausible. Only when considering data from Mars also does it become apparent that this can not have been the case due to the arrival times and amplitudes at the two planets. Comparing the red and black lines in Figure 4 at Earth, we see how similar an ICME with an initial speed of 844 km s^{-1} which hits Earth fairly square on can look to an ICME with an initial speed of 1200 km s^{-1} which only grazes Earth (in the work given by *Falkenberg et al.* [2010] it is also shown how the effects of changing one input parameter in ENLIL is sometimes easily equalled or canceled by changing another parameter when only using single point validation). This exercise underlines the need for multipoint observations when investigating CMEs/ICMEs.

[38] The large discrepancy in the initial longitudinal direction of the CME between the interpretations of the SOHO/LASCO images using the XOL method and the analysis of the multipoint data (~36°) can have several explanations. The XOL method builds on 2-D images of a 3-D structure, and assumes the CME propagates in a perfectly cone shaped manner moving in a straight line radially from the Sun. CMEs are generally not uniform structures propagating in a nice cone-shaped manner, and though this is the best current approximation, the subject still requires further studies, which are not the purpose of this paper. If the CME propagation deviates from the cone shape (which it likely does), or one side of the CME propagates faster than another, then this will give fairly large errors in the initial direction, width and speed of the CME [*Vršnak et al.*, 2007]. If the ICME is deflected either in longitudinal or latitudinal direction as has been demonstrated for previous events [e.g., *Wang et al.*, 2006; *Liu et al.*, 2010; *Byrne et al.*, 2010], this will also give a rather large error in these parameters. One can also imagine that a narrow 3-D structure moving rapidly towards Earth would look very similar to a broad slow structure moving towards (or away from) the Earth in the images. Another factor is the fact that the ICMEs in ENLILv2.6 do not carry a magnetic cloud. Several papers [*Wang et al.*, 2004, 2006; *Shen et al.*, 2009] show that ICMEs can be deflected in the longitudinal direction by the spiral structure of the solar wind. In particular they find that fast ICMEs in some cases can be deflected ~30° in the same direction as the spiral structure of the solar wind, not too far from the 36° deflection with the spiral structure we have introduced here for ICME1. See in particular the illustrations of *Wang et al.* [2004, Figure 4, 2006, Figure 6]. ENLILv2.6 allows for an asymmetric development of the ICME as seen in Figure 5. This is due to different drag effects on different parts of the ICME shock front and features in the background solar wind, which could, in fact, be the process at work in the observed deflection of ICMEs. As intense flares and fast and massive CMEs are usually related and the CME in question presumably was related to the M2.8 flare at E42, the CME may have originated from the same region [e.g., *Vršnak et al.*, 2007; *Temmer et al.*, 2009]. The good results of the longitudinal shift, which corresponds to E50, in the modified ENLILv2.6 run therefore seems indicate an error in the estimation of direction from the SOHO/LASCO images, or perhaps a combination of this and deflection.

[39] The discrepancy between the data and the initial ENLILv2.6 runs may also, in part, be due to structure in the ICME front, which is not built into the input of ENLILv2.6 [*Falkenberg et al.*, 2010, Figure 1], as it is in, eg., HAFv.2-3D MHD [*Intriligator et al.*, 2005; *Wu et al.*, 2007].

[40] The time period studied here provides an opportunity to study two very different SEP events present at both Earth and Mars, allowing investigating of the importance of magnetic connection to the origin of the flare responsible for the SEPs. On 22 November we see the effects of two intense flares. The first of the two flares seemed to miss Mars but hit Earth, the flare site being ~34° west of theoretical ideal magnetic connection to Mars and ~11° west of ideal connection to Earth, while the second flare (~3° west of ideal connection to Mars and ~22° east of ideal connection to Earth) is seen clearly at both planets. We also see a SEP event related to the CME and perhaps also the very eastern flare on 17 November, which is a significant SEP event on Mars, presumably because Mars is hit by the bulk of the ICME, but is almost negligible at Earth (especially in the

high energy range >30 MeV) as the ICME only grazed Earth. Modeling of SEP events would have been very useful in order to determine the most likely origin of particles when several intense flares are present within a relatively short time span. Unfortunately there is not yet a model capable of modeling SEP propagation to Mars. However, A. Aran is working on extending the empirical SOLPENCO code [*Aran et al.*, 2006] to Mars (A. Aran, personal communication, 2009) and J. Luhmann is working on developing an SEP model coupled to the ENLIL and CORHEL models in order to get a shock source of SEPs incorporated in the model as well [*Luhmann et al.*, 2010].

[41] MGS data provide an unforeseen opportunity to study both ICME and SEP events. Arrival times of ICMEs at Mars are obvious in the magnetic pressure proxy from Mars compiled from MGS/MAG measurements (Figure 1). Other phenomena, such as corotating interaction regions, may also cause compression of the magnetosphere at Mars and thereby increased magnetic pressure, however combining MGS/MAG and MGS/ER data, one can see clear shock signatures in both the pressure proxy and the particle/SEP data, enabling certain identification of ICME shock fronts (here represented by the 17 November M2.8 flare and CME). The 7 year time range of MGS data also provides a large baseline of observations and a variety of events having different peak magnetic pressures and ER background count rates. We gain confidence in our method of studying SEPs using the background count rates of MGS/ER from the fact that the SEP profiles from both GOES and MGS/ER look similar in shape and relative magnitude for the 22 November 2001 M9.9 flare. The onset of the SEP event at Mars is also seen to correspond with the flare launch and the onset of the SEP event in GOES data.

[42] Future analysis of MGS data for other events may give us a better understanding of the propagation of ICMEs, longitudinal extent of both ICMEs and SEPs and the relation between flare and CME related SEPs. MGS provides data from the entire period of the last solar maximum where several events could be of high interest to forecasters in the field. The coming of a new solar maximum may provide a new bouquet of larger events to analyze from the current multipoint spacecraft configurations, however we may still learn a lot from closer examination of earlier events. Modeling, especially when SEP modeling starts being available with MHD models, is a good way to find out how accurate our current understanding of ICME propagation is and whether our biggest source of error lies in the assumptions within the models or in our estimates of the initial propagation parameters of the CMEs.

7. Conclusions

[43] We have modeled three CMEs in late November 2001 using the WSAv1.6/ENLILv2.6 3-D MHD code, and investigated the events and their associated flares using solar observations (SOHO/LASCO, GOES) and in situ data from Mars (MGS) and Earth (OMNI, GOES). The focus is on basic parameters important in a space weather context, such as shock arrival time, peak dynamic pressure and SEP profile. We find:

[44] 1. Even using a modern state-of-the-art 3-D full MHD code, multipoint observations are essential to validate modeling of ICME propagation, as two very different ICMEs can look identical if only using one validation point. Multipoint observations can also provide additional knowledge about essential input parameters to the model, eg. in the case presented here where the estimated direction of the ICME was improved through analysis of both Earth and Mars data in conjunction.

[45] 2. The direction of the ICME has been identified as a problematic parameter in prediction of ICME arrival time and amplitude. Two possible errors in determination of the ICME propagation direction have been identified when using current methods to infer ICME initial parameters in combination with the ENLILv2.6 code: (1) The current methods for determination of the initial direction based on SOHO/LASCO images can lead to a significant error in the ICME direction. (2) The ICME can be deflected during propagation and therefore move nonradially. This may not be properly modeled in the ENLILv2.6 code due to the lack of a magnetic cloud, the quality of the input from the WSAv1.6 model using MWO magnetograms or the grid resolution. Tests were made with the highest resolution of ENLILv2.6 available ($1024 \times 120 \times 360$), which did not improve the results significantly.

[46] It is not immediately possible to distinguish between the two, but the results for the 17 November 2001 CME studied here indicate that most likely a combination of the two occurred. It also seems that if the CME in question is related to a flare, the flare position may be a better estimate of the initial direction of the CME in ENLIL, this will be a subject for further study.

[47] 3. Using MGS MAG/ER data in combination with OMNI and GOES data, it was possible to provide a consistent picture of the ICMEs and SEPs both in terms of relative magnitude, arrival times and general profiles for the events studied here. In consequence, MGS MAG/ER measurements could provide useful information in future multipoint studies, using the Martian pressure proxy for ICMEs and the background measurements from the ER instrument for SEPs. This could be very useful for future investigations of space weather on Mars and also for validation of heliospheric models in general.

[48] **Acknowledgments.** All simulations carried out for this work were graciously performed at the Community Coordinated Modeling Center at the NASA Goddard Space Flight Center whose efforts have been invaluable; special thanks to Antti A. Pulkkinen, Anna Chulaki, Larisa Moiseev, and Peter Macneice, and of course to Dusan Odstrcil, also at NASA Goddard Space Flight Center, for developing ENLIL and for letting us use his model in this study. The OMNI database is generously provided and maintained by Goddard Space Flight Centers National Space Science Data Center, thanks to the cooperation and assistance of the many contributing NASA mission investigators. The SOHO/LASCO CME catalog is generated and maintained at the CDAW Data Center by NASA and the Catholic University of America in cooperation with the Naval Research Laboratory. SOHO is a project of international cooperation between ESA and NASA. The GOES X-ray catalogue and the GOES data are generated and maintained by the National Geophysical Data Center (NGDC), located in Boulder, Colorado, part of the U.S. Department of Commerce (USDOC), National Oceanic and Atmospheric Administration (NOAA), National Environmental Satellite, Data and Information Service (NESDIS), one of three NOAA National Data Centers. The research leading to the results presented in this paper has received funding from European Communitys Seventh Framework Programme (FP7/2007-2013) under grant agreement 218816. This study was partially funded by the ESA PRODEX Experiment Arrangement 90322.

[49] Philippa Browning thanks the reviewers for their assistance in evaluating this paper.

References

Aran, A., B. Sanahuja, and D. Lario (2006), SOLPENCO: A solar particle engineering code, *Adv. Space Res.*, *37*, 1240–1246, doi:10.1016/j.asr.2005.09.019.

Arge, C. N., J. G. Luhmann, D. Odstrcil, C. J. Schrijver, and Y. Li (2004), Stream structure and coronal sources of the solar wind during the May 12th, 1997 CME, *J. Atmos. Sol. Terr. Phys.*, *66*, 1295–1309.

Brain, D. A. (2006), Mars Global Surveyor measurements of the Martian solar wind interaction, *Space Sci. Rev.*, *126*, 77–112, doi:10.1007/s11214-006-9122-x.

Brain, D. A., J. S. Halekas, R. Lillis, D. L. Mitchell, and R. P. Lin (2005), Variability of the altitude of the Martian sheath, *Geophys. Res. Lett.*, *32*, L18203, doi:10.1029/2005GL023126.

Brueckner, G. E., et al. (1995), The Large Angle Spectroscopic Coronagraph (LASCO), *Sol. Phys.*, *162*(1–2), 357–402, doi:10.1007/BF00733434.

Burlaga, L., et al. (1980), Interplanetary particles and fields, November 22 to December 6, 1977: Helios, Voyager and Imp observations between 0.6 and 1.6 AU, *J. Geophys. Res.*, *85*, 2227–2242, doi:10.1029/JA085iA05p02227.

Burlaga, L., E. Sittler, F. Mariani, and R. Schwenn (1981), Magnetic loop behind an interplanetary shock: Voyager, Helios, and IMP 8 observations, *J. Geophys. Res.*, *86*, 6673–6684, doi:10.1029/JA086iA08p06673.

Byrne, J. P., S. A. Maloney, R. T. J. McAteer, J. M. Refojo, and P. T. Gallagher (2010), Propagation of an Earth-directed coronal mass ejection in three dimensions, *Nat. Commun.*, *1*, 74, doi:10.1038/ncomms1077.

Cain, J. C., B. B. Ferguson, and D. Mozzoni (2003), An $n = 90$ internal potential function of the Martian crustal magnetic field, *J. Geophys. Res.*, *108*(E2), 5008, doi:10.1029/2000JE001487.

Cremades, H., V. Bothmer, and D. Tripathi (2006), Properties of structured coronal mass ejections in solar cycle 23, *Adv. Space Res.*, *38*, 461–465, doi:10.1016/j.asr.2005.01.095.

Crider, D. H., D. Vignes, A. M. Krymskii, T. K. Breus, N. F. Ness, D. L. Mitchell, J. A. Slavin, and M. H. Acuña (2003), A proxy for determining solar wind dynamic pressure at Mars using Mars Global Surveyor data, *J. Geophys. Res.*, *108*(A12), 1461, doi:10.1029/2003JA009875.

Crider, D. H., J. Espley, D. A. Brain, D. L. Mitchell, J. E. P. Connerney, and M. H. Acuña (2005), Mars Global Surveyor observations of the Halloween 2003 solar super storm's encounter with Mars, *J. Geophys. Res.*, *110*, A09S21, doi:10.1029/2004JA010881.

Cully, C. M., E. F. Donovan, A. W. Yau, and G. G. Arkos (2003), Akebono/Suprathermal Mass Spectrometer observations of low-energy ion outflow: Dependence on magnetic activity and solar wind conditions, *J. Geophys. Res.*, *108*(A2), 1093, doi:10.1029/2001JA009200.

Dennis, B. R., L. Haga, D. A. Medlin, and A. K. Tolbert (2006), Correlated flare and CME energies for the October/November 2003 events, *Bull. Am. Astron. Soc.*, *38*, 232.

Dubinin, E., et al. (2008), Structure and dynamics of the solar wind/ionosphere interface on Mars: MEX-ASPERA-3 and MEX-MARSIS observations, *Geophys. Res. Lett.*, *35*, L11103, doi:10.1029/2008GL033730.

Dryer, M. (1987), Study of Travelling interplanetary Phenomena report, *Sol. Phys.*, *114*, 407–411.

Dryer, M., and M. A. Shea (1986), Scientific highlights of the Study of Travelling Interplanetary Phenomena (STIP) intervals during the SMY/SMA, *Adv. Space Res.*, *6*, 343–351, doi:10.1016/0273-1177(86)90174-2.

Dryer, M., Z. Smith, C. D. Fry, W. Sun, C. S. Deehr, and S.-I. Akasofu (2004), Real-time shock arrival predictions during the "Halloween 2003 epoch," *Space Weather*, *2*, S09001, doi:10.1029/2004SW000087.

Emslie, A. G., B. R. Dennis, G. D. Holman, and H. S. Hudson (2005), Refinements to flare energy estimates: A followup to "Energy partition in two solar flare/CME events" by A. G. Emslie et al., *J. Geophys. Res.*, *110*, A11103, doi:10.1029/2005JA011305.

Espley, J. R., P. A. Cloutier, D. H. Crider, D. A. Brain, and M. H. Acuña (2005), Low-frequency plasma oscillations at Mars during the October 2003 solar storm, *J. Geophys. Res.*, *110*, A09S33, doi:10.1029/2004JA010935.

Falkenberg, T. V., B. Vršnak, A. Taktakishvili, D. Odstrcil, P. MacNeice, and M. Hesse (2010), Investigations of the sensitivity of a coronal mass ejection model (ENLIL) to solar input parameters, *Space Weather*, *8*, S06004, doi:10.1029/2009SW000555.

Filippov, B. P., N. Gopalswamy, and A. V. Lozhechkin (2001), Non-radial motion of eruptive filaments, *Sol. Phys.*, *203*, 119–130, doi:10.1023/A:1012754329767.

Futaana, Y., et al. (2008), Mars Express and Venus Express multi-point observations of geoeffective solar flare events in December 2006, *Planet. Space Sci.*, *56*, 873–880, doi:10.1016/j.pss.2007.10.014.

Heras, A. M., B. Sanahuja, Z. K. Smith, T. Detman, and M. Dryer (1991), On the large-scale effects of two interplanetary shocks on the associated paticle events, *J. Atmos. Terr. Phys.*, *53*, 1033-1038.

Intriligator, D. S., W. Sun, M. Dryer, C. D. Fry, C. Deehr, and J. Intriligator (2005), From the Sun to the outer heliosphere: Modeling and analyses of the interplanetary propagation of the October/November (Halloween) 2003 solar events, *J. Geophys. Res.*, *110*, A09S10, doi:10.1029/2004JA010939.

Jackson, B. V., J. A. Boyer, P. P. Hick, A. Buffington, M. M. Bisi, and D. H. Crider (2007), Analysis of solar wind events using interplanetary scintillation remote sensing 3D reconstructions and their comparison at Mars, *Sol. Phys.*, *241*, 385–396, doi:10.1007/s11207-007-0276-9.

Kilpua, E. K. J., J. Pomoell, A. Vourlidas, R. Vainio, J. Luhmann, Y. Li, P. Schroeder, A. B. Galvin, and K. Simunac (2009), STEREO observations of interplanetary coronal mass ejections and prominence deflection during solar minimum period, *Ann. Geophys.*, *27*, 4491–4503.

Klein, K. L., E. L. Chupp, G. Trottet, A. Magun, P. P. Dunphy, E. Rieger, and S. Urpo (1999), Flare-associated energetic particles in the corona and at 1 AU, *Astron. Astrophys. Trans.*, *348*, 271–285.

Lee, C. O., J. G. Luhmann, D. Odstrcil, P. J. MacNeice, I. de Pater, P. Riley, and C. N. Arge (2009), The solar wind at 1 AU during the declining phase of solar cycle 23: Comparison of 3D numerical model results with observations, *Sol. Phys.*, *254*, 155–183, doi:10.1007/s11207-008-9280-y.

Liu, Y., J. A. Davies, J. G. Luhmann, A. Vourlidas, S. D. Bale, and R. P. Lin (2010), Geometric triangulation of imaging observations to track coronal mass ejections continuously out to 1 AU, *Astrophys. J.*, *710*, L82–L87, doi:10.1088/2041-8205/710/1/L82.

Lugaz, N., J. N. Hernandez-Charpak, I. I. Roussev, C. J. Davis, A. Vourlidas, and J. A. Davies (2010), Determining the azimuthal properties of coronal mass ejections from multi-spacecraft remote-sensing observations with STEREO SECCHI, *Astrophys. J.*, *715*, L493–L499, doi:10.1088/0004-637X/715/1/493.

Luhmann, J. G., S. A. Ledvina, D. Odstrcil, M. J. Owens, X.-P. Zhao, Y. Liu, and P. Riley (2010), Cone model-based SEP event calculations for applications to multipoint observations, *J. Adv. Space Res.*, *46*, 1–21, doi:10.1016/j.asr.2010.03.011.

McKenna-Lawlor, S. M. P., et al. (2008), Predicting interplanetary shock arrivals at Earth, Mars, and Venus: A real-time modeling experiment following the solar flares of 5–14 December 2006, *J. Geophys. Res.*, *113*, A06101, doi:10.1029/2007JA012577.

Möstl, C., C. J. Farrugia, M. Temmer, C. Miklenic, and A. M. Veronig (2009), Linking remote imagery of a coronal mass ejection to its in situ signatures at 1 AU, *Astrophys. J.*, *705*, L180–L185, doi:10.1088/0004-637X/705/2/L180.

Odstrcil, D., and V. J. Pizzo (1999), Distortion of the interplanetary magnetic field by three-dimensional propagation of coronal mass ejections in a structured solar wind, *J. Geophys. Res.*, *104*, 28,225–28,239, doi:10.1029/1999JA900319.

Odstrcil, D., P. Riley, and X. P. Zhao (2004), Numerical simulation of the 12 May 1997 interplanetary CME event, *J. Geophys. Res.*, *109*, A02116, doi:10.1029/2003JA010135.

Pomoell, J., R. Vainio, and E. K. J. Kilpua (2010), Observation-based analysis of the deflection of a polar crown filament eruption, *AIP Conf. Proc.*, *1216*, 335–338, doi:10.1063/1.3395868.

Pulkkinen, A., T. Oates, and A. Taktakishvili (2009), Automatic determination of the conic coronal mass ejection model parameters, *Sol. Phys.*, *261*, 115–123, doi:10.1007/s11207-009-9473-z.

Reames, D. V. (1999), Particle acceleration at the Sun and in the heliosphere, *Space Sci. Rev. 90*, 413–491.

Schwenn, R., A. Dal Lago, E. Huttunen, and W. D. Gonzalez (2005), The association of coronal mass ejections with their effects near the Earth, *Ann. Geophys.*, *23*, 1033–1059.

Shen, C., Y. Wang, J. Zhang, P. Ye, and S. Wang (2009), The kinematic evolution of the 2007 October CME in the inner corona, *Bull. Am. Astron. Soc.*, *41*, 856.

Smith, Z., and M. Dryer (1990), MHD study of temporal and spatial evolution of simulated interplanetary shocks in the ecliptic plane within 1 AU, *Sol. Phys.*, *129*, 387–405.

Smith, Z., and M. Dryer (1991), Numerical simulations of high-speed solar wind streams within 1 AU and their signatures at 1 AU, *Sol. Phys.*, *131*, 363–383.

Taktakishvili, A., M. Kuznetsova, P. MacNeice, M. Hesse, L. Rastaätter, A. Pulkkinen, A. Chulaki, and D. Odstrcil (2009), Validation of the coronal mass ejection predictions at the Earth orbit estimated by ENLIL

heliosphere cone model, *Space Weather*, *7*, S03004, doi:10.1029/2008SW000448.

Temmer, M., S. Preiss, and A. M. Veronig (2009), CME projection effects studied with STEREO/COR and SOHO/LASCO, *Sol. Phys.*, *256*, 183–199, doi:10.1007/s11207-009-9336-7.

Vennerstrom, S., N. Olsen, M. Purucker, M. H. Acuña, and J. C. Cain (2003), The magnetic field in the pile-up region at Mars and its variation with the solar wind, *Geophys. Res. Lett.*, *30*(7), 1369, doi:10.1029/2003GL016883.

von Rosenvinge, T., I. Richardson, D. Reames, C. Cohen, A. Cummings, R. Leske, R. Mewaldt, E. C. Stone, and M. Wiedenbeck (2009), The solar energetic particle event of December 14, 2006, *Sol. Phys.*, *256*, 443–462.

Vršnak, B., and N. Gopalswamy (2002), Influence of the aerodynamic drag on the motion of interplanetary ejecta, *J. Geophys. Res.*, *107*(A2), 1019, doi:10.1029/2001JA000120.

Vršnak, B., D. Sudar, D. Ruždjak, and T. Žic (2007), Projection effects in coronal mass ejections, *Astron. Astrophys.*, *469*, 339–346, doi:10.1051/0004-6361/20077175.

Vršnak, B., T. Žic, T. V. Falkenberg, C. Möstl, S. Vennerstrom, and D. Vrbanec (2010), The role of aerodynamic drag in propagation of interplanetary coronal mass ejections, *Astron. Astrophys.*, *512*, A43, doi:10.1051/0004-–6361/200913482.

Wang, Y., C. Shen, S. Wang, and P. Ye (2004), Deflection of coronal mass ejection in the interplanetary medium, *Sol. Phys.*, *222*, 329–343, doi:10.1023/B:SOLA.0000043576.21942.aa.

Wang, Y., X. Xue, C. Shen, P. Ye, S. Wang, and J. Zhang (2006), Impact of major coronal mass ejections on geospace during 2005 September 7–13, *Astrophys. J.*, *646*, 625–633.

Webb, D., B. Jackson, P. Hick, R. Schwenn, V. Bothmer, and D. Reames (1993), Comparison of CMEs, magnetic clouds, and bidirectionally streaming proton events in the heliosphere using helios data, *Adv. Space Res.*, *13*, 71–74, doi:10.1016/0273-1177(93)90459-O.

Wei, F., and M. Dryer (1991), Propagation of solar flare-associated interplanetary shock waves in the heliospheric meridional plane, *Sol. Phys.*, *132*, 373–394.

Wu, C. C., C. D. Fry, S. T. Wu, M. Dryer, and K. Liou (2007), Three-dimensional global simulation of interplanetary coronal mass ejection propagation from the Sun to the heliosphere: Solar event of 12 May 1997, *J. Geophys. Res.*, *112*, A09104, doi:10.1029/2006JA012211.

Xie, H., L. Ofman, and G. Lawrence (2004), Cone model for halo CMEs: Application to space weather forecasting, *J. Geophys. Res.*, *109*, A03109, doi:10.1029/2003JA010226.

Yashiro, S., S. Akiyama, N. Gopalswamy, and R. A. Howard (2006), Different power-law indices in the frequency distributions of flares with and without coronal mass ejections, *Astrophys. J.*, *650*, L143–L146.

Zhang, T. L., J. G. Luhmann, and C. T. Russell (1991), The magnetic barrier at Venus, *J. Geophys. Res.*, *96*, 11,145–11,153.

Zhao, X. H., X. S. Feng, C. Q. Xiang, Y. Liu, Z. Li, Y. Zhang, and S. T. Wu (2010), Multi-spacecraft observations of the 2008 January 2 CME in the inner heliosphere, *Astrophys. J.*, *714*, 1133–1141, doi:10.1088/0004-637X/714/2/1133.

D. A. Brain and G. Delory, Space Sciences Laboratory, University of California, Berkeley, CA 94720, USA. (brain@ssl.berkeley.edu; gdelory@ssl.berkeley.edu)

T. V. Falkenberg and S. Vennerstrom, National Space Institute, Danish Technical University, Lyngby DK-2100, Denmark. (tvf@space.dtu.dk; sv@space.dtu.dk)

A. Taktakishvili, NASA Goddard Space Flight Center, Greenbelt, MD 20771, USA. (aleksandre.taktakishvili-1@nasa.gov)